JOURNAL OF MATERIALS SCIENCE 30 (1995) 5960–5966

Characterization of 6FDA–APBP polyimide films through impulsive stimulated thermal scattering

J. K. COCSON, C. S. HAU, P. M. LEE, C. C. POON, A. H. ZHONG, J. A. ROGERS, K. A. NELSON
Department of Chemistry, Massachusetts Institute of Technology, Cambridge, MA 02139, USA

The elastic and thermal properties of 4,4′-(hexafluoroisopropylidene)-*bis* (phthalic anhydride)-4,4′-*bis*(4-aminophenoxy) biphenyl (6FDA–APBP) free-standing polyimide films (2–10 μm) were investigated using impulsive stimulated thermal scattering (ISTS), a non-contact optical method for thin film characterization. Shear and longitudinal velocities, Young's modulus, Poisson's ratio and the in-plane thermal diffusivity are reported.

1. Introduction

In recent decades, polymer thin films have become increasingly important in microelectronics, automotive, aerospace, magnetic disk and many other applications. In most cases, accurate quantitative characterization of polymer films is crucial. However, *in situ* measurement of mechanical and thermal transport properties is often difficult or time consuming. Measurements may be restricted to special test samples rather than actual finished devices. In addition, characterization of polymer films during, as well as after, fabrication would be extremely useful for process monitoring and refinement of fabrication procedures. This has not been possible for mechanical or thermal properties, in general. In a series of recent papers [1–6], a laser-based ultrasonic method known as impulsive stimulated thermal scattering (ISTS) has been introduced for fast, non-invasive, non-contact *in situ* evaluation of thin films. In ISTS, two short excitation laser pulses are crossed spatially and temporally in the film sample to create a sinusoidally varying interference or "grating" pattern. This gives rise to sudden ("impulsive") heating and thermal expansion with the same spatially periodic geometry. The resulting acoustic and thermal responses of the sample are observed by monitoring the time-dependent diffraction of a probe laser beam off the generated material grating. ISTS studies of supported and unsupported polymer films, including anisotropic films and films undergoing cure, have been reported. In addition, "hard" films including ferroelectric ceramics, diamond-like carbon, carbon nitride and others have been examined.

In this paper we report the results of an ISTS investigation of a series of free-standing films of the polyimide 4,4′-(hexafluoroisopropylidene)-*bis*(phthalic anhydride)-4,4′-*bis*(4-aminophenoxy) biphenyl (6FDA–APBP, commercially known as Amoco UD4212) with thicknesses in the 2–10 μm range. Elastic properties, namely the shear and longitudinal velocities, Young's modulus and Poisson's ratio, are determined. Also reported is the in-plane thermal diffusivity. The samples were checked for mechanical anisotropy and for any variation of the properties with film thickness.

2. Experimental procedure

The samples consisted of two sets of spin-coated and fully cured UD4212 (6FDA–APBP) on 3 and 4 inch diameter silicon wafers. The chemical structure of the polyimide is shown in Fig. 1. Curing was performed in a temperature-regulated oven under a N_2 atmosphere using the schedule described in Table I [7]. Six of the samples were fabricated at MIT and 12 at Amoco. The MIT films had thicknesses of 3.93, 4.00, 5.01, 6.96, 7.44 and 9.76 ± 0.05 μm and the Amoco films had thicknesses of 2.86, 2.99, 3.97, 4.93, 5.83, 6.68, 6.98, 7.60, 7.97, 8.88, 8.97 and 9.88 ± 0.05 μm, as measured with a mechanical stylus profilometer (DEKTAK 8000). As described in Refs 8–10, two 1 inch regions in each of the wafers were etched away with a solution mixture of 6:1:1 hydrofluoric acid:nitric acid:acetic acid, leaving unsupported regions of the polymer films.

The ISTS experimental set-up is shown schematically in Fig. 2. Two 355 nm excitation laser pulses derived from a Q-switched, mode-locked and cavity-dumped Nd: YAG laser (modified Series 520 Control Laser) were crossed spatially and temporally at the film surface. Interference between the excitation pulses produced a grating intensity pattern characterized by a wavevector $\boldsymbol{q}$ of magnitude

$$q = \frac{4\pi\sin(\theta/2)}{\lambda_L} = \frac{2\pi}{\Lambda} \quad (1)$$

where λ_L is the laser wavelength, θ is the angle between the excitation pulses and Λ is the grating fringe spacing. Light absorption led to sudden formation of

0022–2461

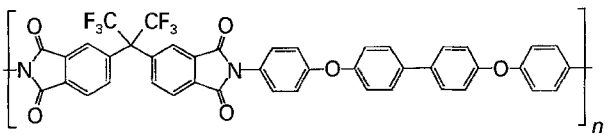

Figure 1 Chemical structure of 6FDA–APDP.

TABLE I Cure schedule for UD4212 thin films in nitrogen [7]

	Temperature (°C)	Time (min)
Soft cure	140	30 hold
Hard cure	100–200	30 ramp
	200	30 hold
	200–400	10 ramp
	400	60 hold

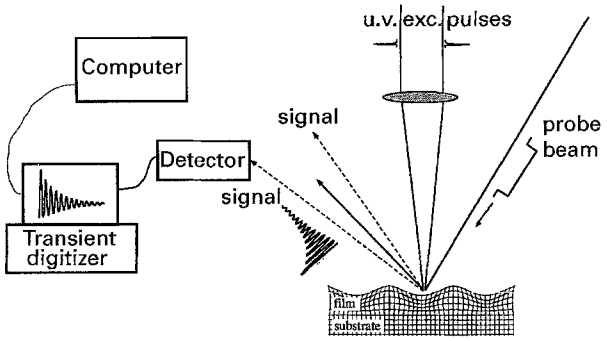

Figure 2 Experimental set-up for real-time ISTS experiments on thin films. Two excitation pulses are crossed at the film surface, overlapping spatially and temporally with a probe laser beam generated by an argon ion laser. The diffracted signal is time-resolved with a photodiode and a transient recorder.

a temperature grating which imaged the optical interference pattern. Thermal expansion then launched acoustic and thermal responses with wavevectors $\pm q$. These responses resulted in spatially periodic modulation ("ripple") of the film surface, which acted as a diffraction grating. Damped acoustic oscillations and thermal diffusion were monitored directly through measurement of the time-dependent diffraction of a probe laser beam [2, 11].

The probe beam was derived from a c.w. argon ion laser (Coherent Innova 70-4, 1W, single frequency, 514 nm) equipped with an electro-optic gate (Con-Optics Model 3) to yield a square pulse with an adjustable temporal width. The diffracted signal was monitored with a fast photodiode (Antel ARX-SA) and transient digitizing oscilloscope (Tektronix DSA 602A).

Data were collected at crossing angles of 0.733, 0.825, 1.05, 1.24, 1.25, 1.51, 1.59, 1.75, 2.02, 2.30, 2.32, 2.69, 2.80, 2.88, 3.05, 3.23, 3.59, 3.82, 3.85 and 3.99 $\pm$ 0.05°. The angles were measured using a mechanical rotation stage.

3. Results

3.1. ISTS data: Qualitative description

Typical ISTS data from the 5.01 and 7.44 μm samples, recorded at two different crossing angles, are shown in Fig. 3. The material response consisted of damped acoustic oscillations observed on a nanosecond timescale followed by thermal diffusion observed on a microsecond timescale. As the wavevector magnitude q was varied by changing the scattering angle, both responses changed. Thermal diffusion between grating peaks and nulls became faster as the grating period became smaller, i.e. at higher q. The acoustic response changed not only quantitatively, as discussed below in terms of acoustic frequencies and velocities, but qualitatively in that the number and type of acoustic modes which were observed were wavevector dependent. This is apparent from the Fourier transforms of the data in Fig. 3, which show the acoustic mode frequencies. The q-dependent behaviour has been discussed in detail previously [1, 2]. Briefly, when the acoustic wavelength is comparable to or less than the film thicknesses, the film acts as an acoustic waveguide which supports many acoustic modes called Lamb modes [12, 13]. This is in contrast to the behaviour of a bulk isotropic material in which there are only three acoustic modes, two transverse and one longitudinal, for each wavevector. The bulk limit is reached when the acoustic wavelength becomes very short compared to the film thickness. In the waveguide regime (unlike the bulk case), the acoustic velocity varies sharply with wavevector magnitude. In particular, the velocity of each mode depends on the ratio of the acoustic wavelength, Λ, to the film thickness, d, i.e. on the product qd. The velocity also depends on the elastic properties of the film, i.e. the bulk shear and longitudinal acoustic velocities. The velocity and its dispersion with wavevector can be mapped out through ISTS measurements with different crossing angles. From the results, the elastic properties can be determined [2].

3.2. Acoustic signal and data analysis

From the acoustic frequencies, ω, and the wavevector magnitudes, q, the phase velocities, $v = \omega/q$, for each mode observed at each wavevector are determined. The acoustic velocities of the two lowest-order modes were used to determine the elastic properties through a non-linear least-squares fitting algorithm. The values determined in this manner were then used to calculate the velocity dispersion curves of the first eight acoustic waveguide modes. The measured phase velocities are shown as a function of qd along with the best-fit calculated dispersion curves in Fig. 4a (MIT samples) and b (Amoco samples). The fits and calculated curves are based on an isotropic model of a stressed unsupported film [14]. The values of the elastic moduli were not sensitive to the residual stress values, which were in the 30–60 MPa range and were only determined to within $\pm$50% uncertainties. More precise residual stress determination would require measurements at smaller qd values [14]. The fits indicate that there is no significant anisotropy in the film moduli.

In Fig. 5, dispersion results from all of the MIT (Fig. 5a) and Amoco (Fig. 5b) samples are plotted. It is

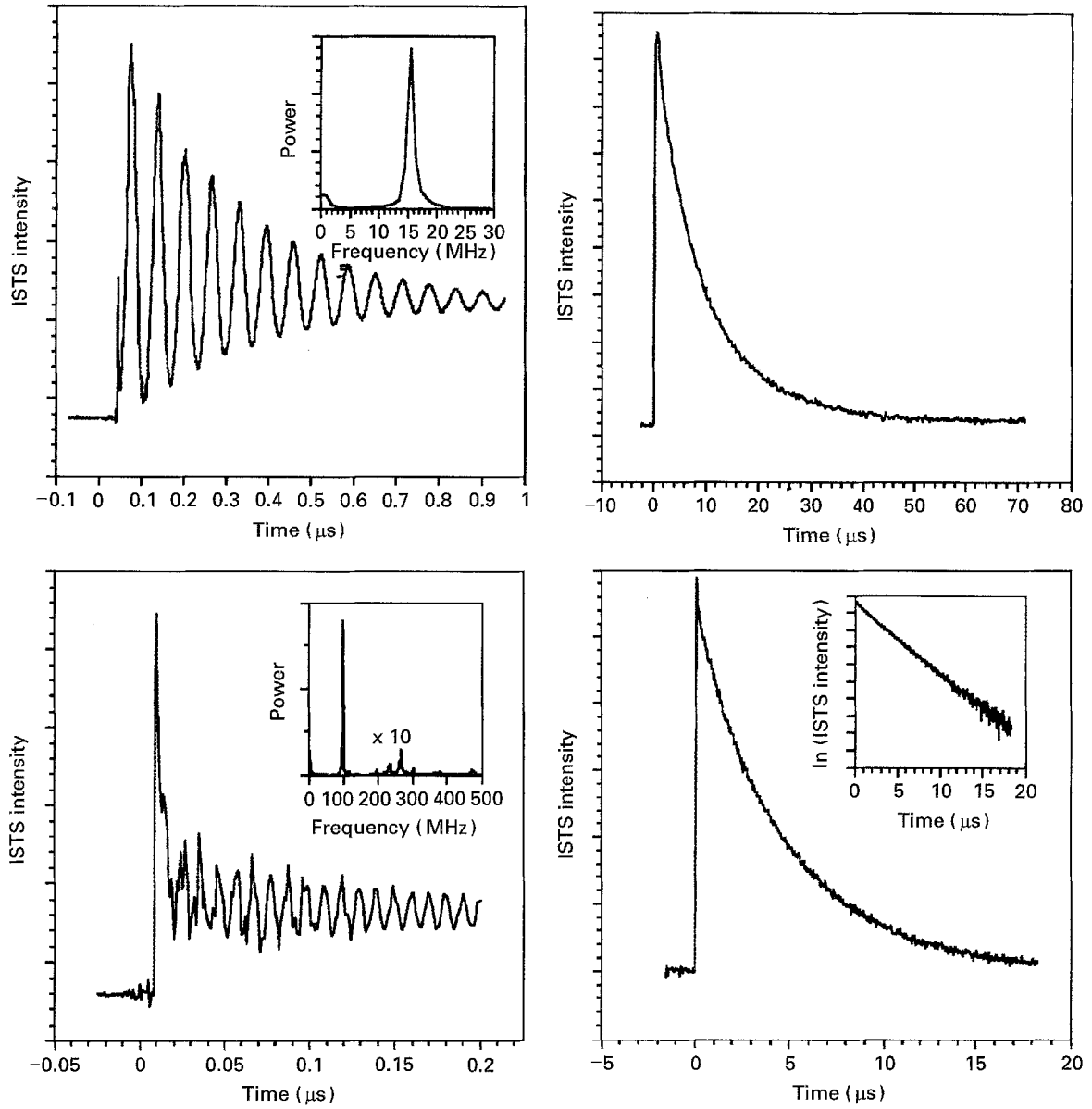

Figure 3 Diffracted ISTS signals from 5.01 (upper frames) and 7.44 μm (lower frames) unsupported UD4212 films with grating wavelengths of 27.7 and 8.84 μm, respectively. The data are the result of 100 averages and were acquired over a time of several seconds. The left-hand frames depict acoustic oscillations and damping while the right-hand frames show the subsequent thermal decays. The upper left-hand acoustic oscillation pattern suggests that only one Lamb acoustic mode is excited in the 5.01 μm film at the excitation wavevector used. The lower left-hand oscillation pattern and power spectrum (inset) reveal several acoustic modes in the 7.44 μm film at the excitation wavevector used. A typical logarithmic plot of the thermal diffusivity data is shown in the lower right-hand frame (inset).

apparent that the velocities measured at many q values from films of different thicknesses, d, scale with the qd product. This indicates that the elastic properties show no systematic thickness dependence. The longitudinal and shear velocities obtained from the curves fit to all the data in Fig. 5a and b are within uncertainties of the velocities obtained from the fits of data from samples of each thickness individually. Table II shows the shear and longitudinal velocities for each thickness and for the combination of all samples in each of the two sets.

From the shear and longitudinal velocities obtained (c_s and c_L, respectively) and from the known film density ($\rho = 1.1\ g\,cm^{-3}$) [15], Young's modulus, $E = 9K\mu/(3K + \mu)$, and Poisson's ratio, $\sigma = (3K - 2\mu)/(6K + 2\mu)$, can be determined for each thickness, and for the combination of all samples in a set. In these equations, K and μ are the bulk and shear moduli, respectively, and are related to c_s, c_L and ρ by: $c_L = [(3K + 4\mu)/\rho]^{1/2}$ and $c_s = (\mu/\rho)^{1/2}$ [16]. As can be seen in Table II, these values are consistent within a set. Uncertainties of $\pm$ 2% for the shear velocity and $\pm$ 5% for the longitudinal velocity are determined using the 90% F-test.

3.3. Thermal diffusion

The decay of signal on microsecond timescales is due to thermal diffusion within the film plane, between the grating peaks and nulls, and perpendicular to the film plane, both into the depth of the film (since the light intensity, and therefore the heating, is greatest at the front surface) and into the surrounding air. In general, the time dependence of diffraction efficiency governed

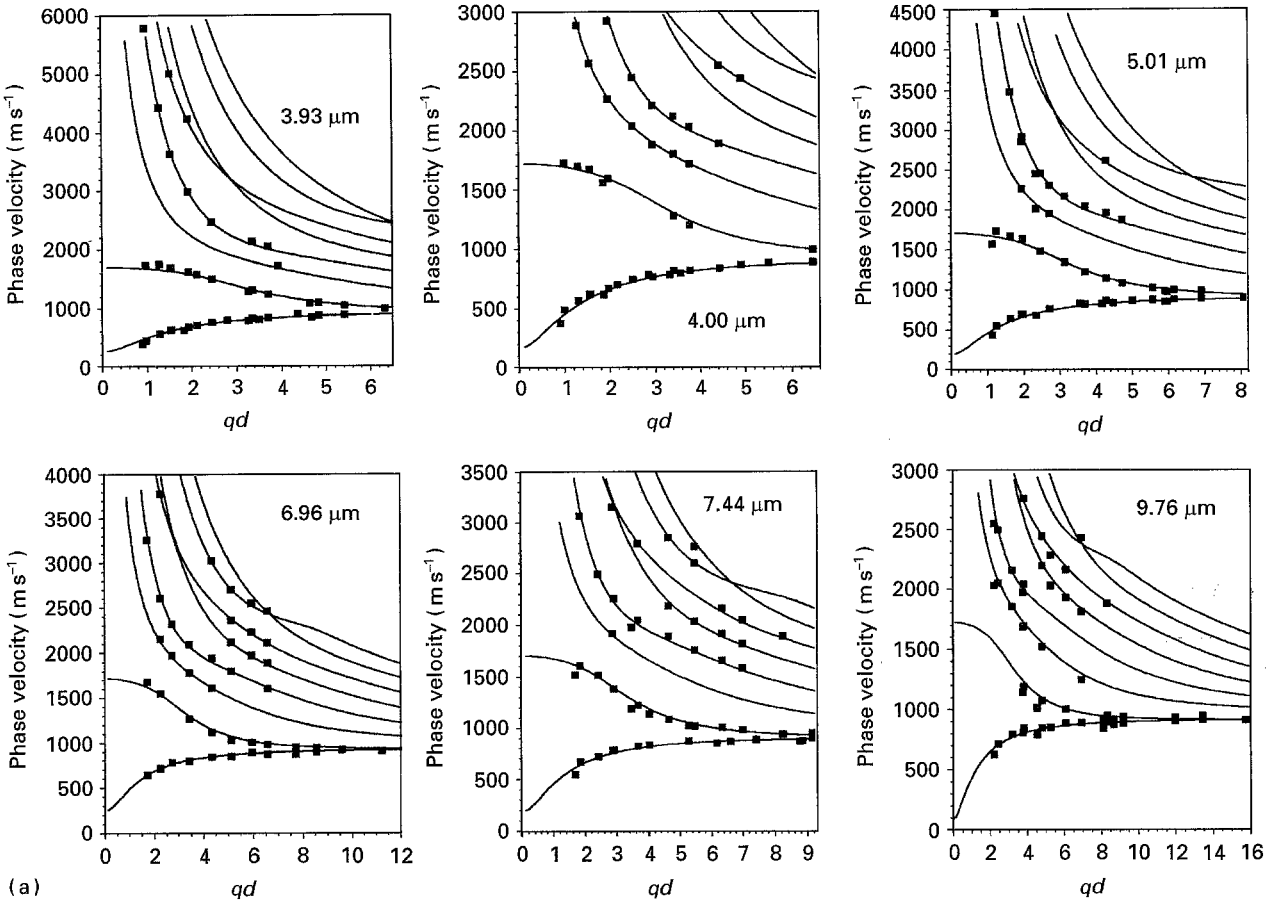

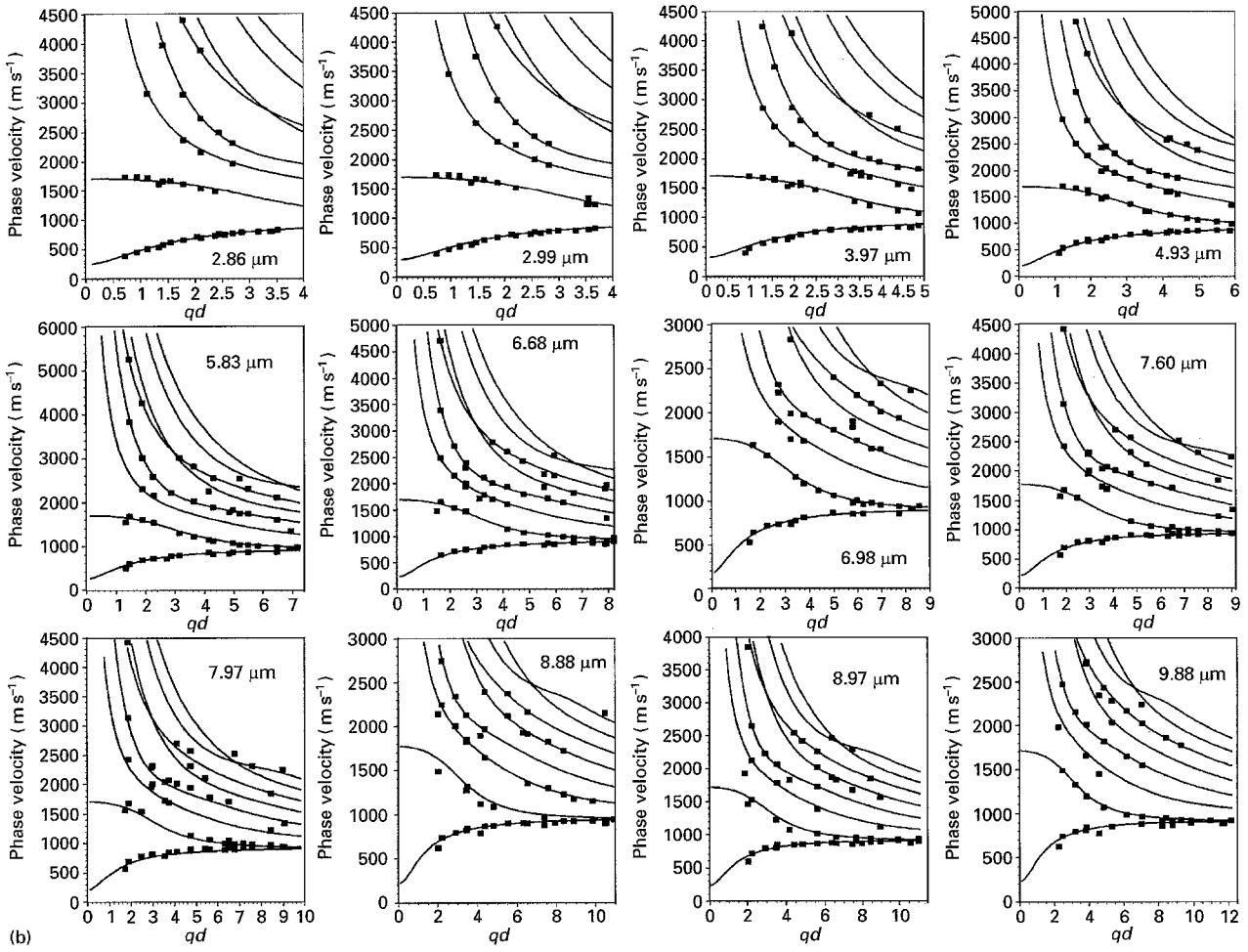

Figure 4 Measured acoustic velocities (symbols) and best-fit calculated dispersion curves in UD4212 unsupported films of various thicknesses fabricated at MIT (a) and Amoco (b). The fits were calculated using an isotropic model of a stressed unsupported film.

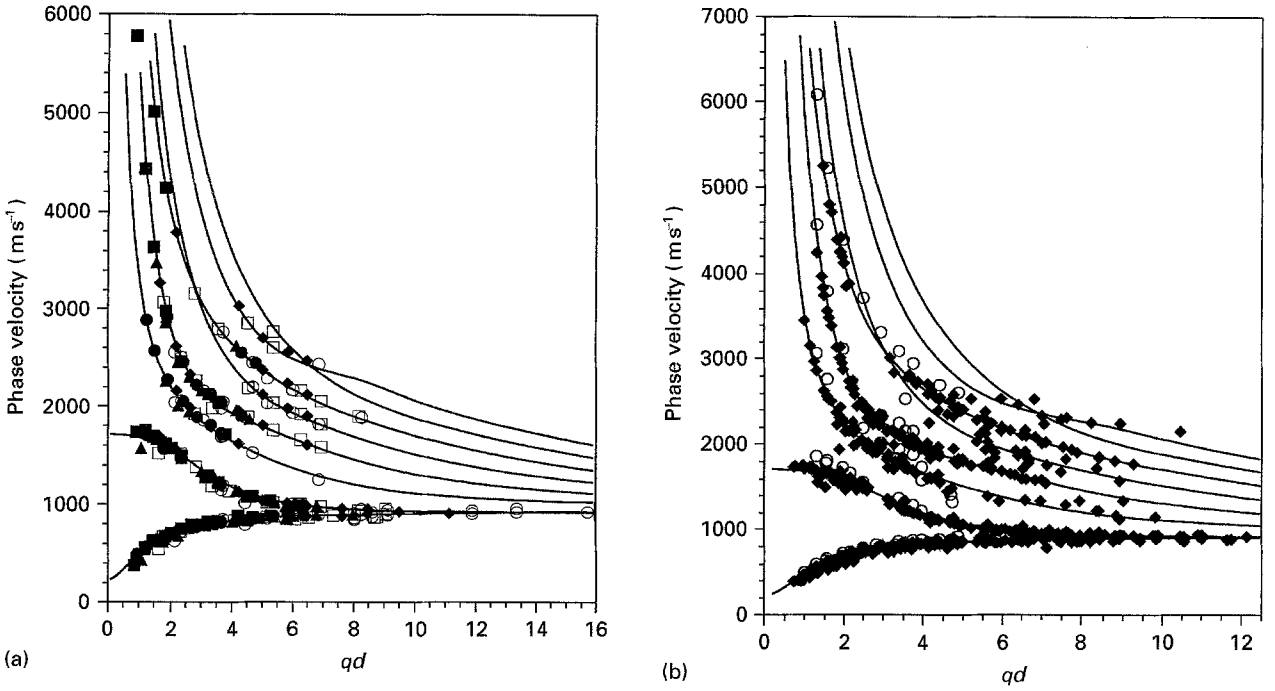

Figure 5 Measured acoustic velocities (symbols) and best-fit calculated dispersion curves in UD4212 unsupported films of various thicknesses fabricated at MIT (a) and Amoco (b). The fits were calculated using an isotropic model of a stressed unsupported film. The good agreement between fits and data from films of different thicknesses indicates that the acoustic velocities scale with qd and therefore that the elastic properties of the thin films scale are thickness independent. In (b), the data points represented by ○ belong to a 3.97 μm unsupported film whose elastic properties (but not thermal diffusivity) appear to be significantly different from the other 12 samples. Thickness of films in (a) (μm) : ■, 3.93; ●, 4.00; ▲, 5.01; ◆, 6.96; □, 7.44; ○, 9.76.

TABLE II Summary of elastic and thermal properties determined from ISTS measurements in unsupported UD4212 thin films

Sample thickness (± 0.05 μm)	Shear velocity (± 20 m s^{-1})	Longitudinal velocity (m s^{-1})	Young's modulus (± 0.3 GPa)	Poisson's ratio (± 0.03)	In-plane thermal diffusivity (μm^2 μs^{-1})
UD4212 fabricated at MIT					
3.93	930	2160 ± 110	2.6	0.39	0.171 ± 0.005
4.00	950	2180 ± 110	2.8	0.38	0.170 ± 0.004
5.01	940	2170 ± 110	2.7	0.39	0.171 ± 0.005
6.96	940	2180 ± 110	2.7	0.38	0.192 ± 0.005
7.44	940	2170 ± 110	2.7	0.39	0.163 ± 0.006
9.76	940	2150 ± 110	2.7	0.38	0.172 ± 0.005
All samples	940	2170 ± 110	2.7	0.38	NA
UD4212 fabricated at Amoco					
2.86	950	2080 ± 100	2.7	0.37	0.120 ± 0.006
2.99	940	2090 ± 100	2.7	0.37	0.126 ± 0.010
3.97	940	2080 ± 100	2.7	0.37	0.147 ± 0.003
4.93	940	2140 ± 110	2.7	0.38	0.173 ± 0.004
5.83	930	2150 ± 110	2.6	0.38	0.188 ± 0.004
6.68	940	2150 ± 110	2.7	0.38	0.185 ± 0.004
6.98	940	2200 ± 110	2.7	0.39	0.183 ± 0.005
7.60	980	2230 ± 110	2.9	0.38	0.186 ± 0.005
7.97	940	2150 ± 110	2.7	0.38	0.180 ± 0.004
8.88	980	2240 ± 110	2.9	0.38	0.191 ± 0.005
8.97	940	2160 ± 110	2.7	0.38	0.191 ± 0.005
9.88	940	2180 ± 110	2.7	0.39	0.166 ± 0.005
All samples	940	2140 ± 110	2.7	0.38	NA

by thermal diffusion can be described by [17]

$$\eta(t) = f^2(t) \exp(-2D_T q^2 t) \quad (2)$$

where $f(t)$ describes the heat flow in the out-of-plane direction and is a complicated function of excitation light absorption length, out-of-plane thermal diffusivity, rate of heat flow from film to surroundings and material parameters associated with signal generation. D_T is the in-plane thermal diffusivity and q is the magnitude of the excitation wavevector (Equation 1).

At large wavevector magnitudes corresponding to short peak–null distances, the decay is dominated by in-plane thermal diffusion, i.e. the second part of

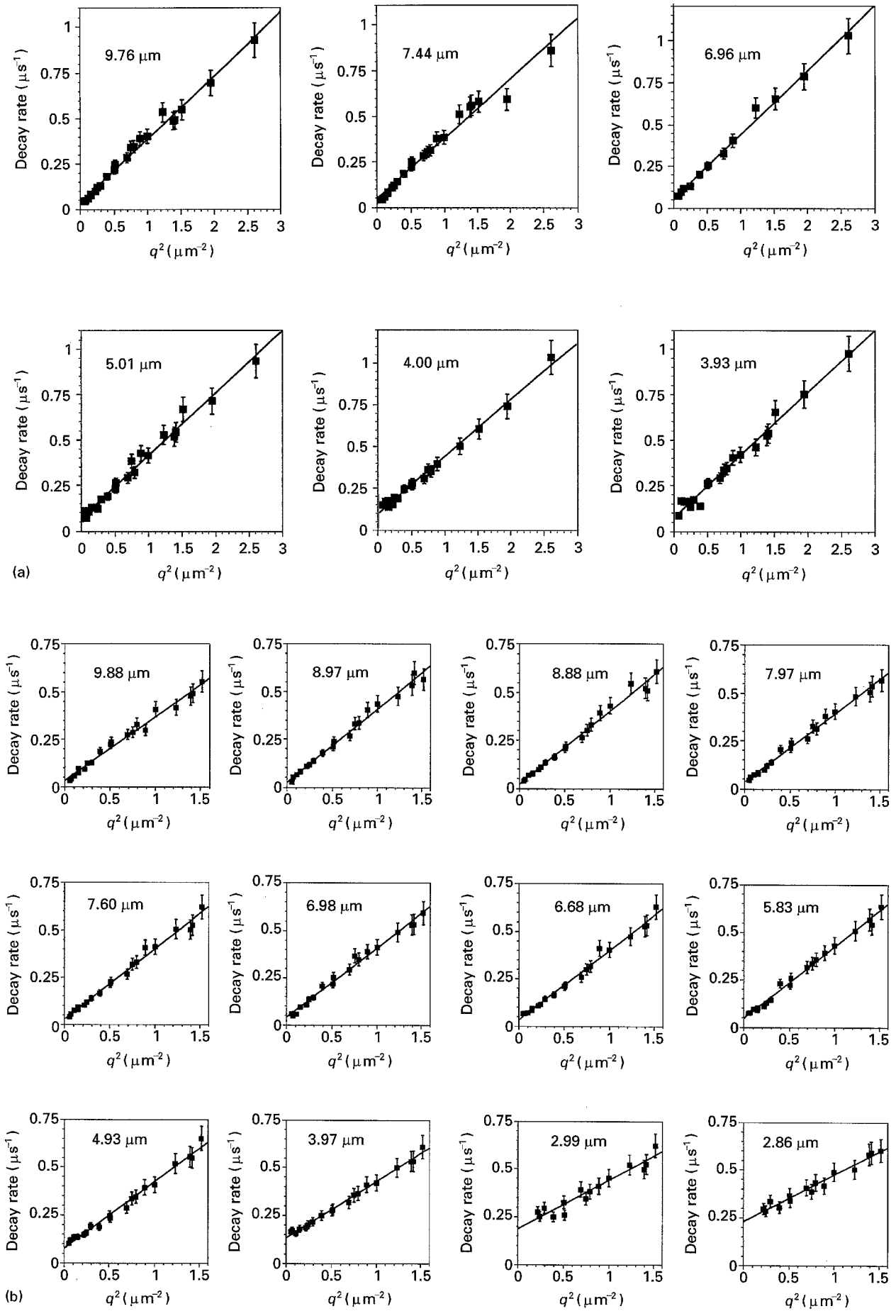

Figure 6 Measured thermal signal decay rates as a function of the excitation wavevectors squared for UD4212 polyimide films fabricated at MIT (a) and Amoco (b). The in-plane thermal diffusivities are found by halving the slopes of the lines. With one exception, the MIT samples show thermal diffusivity values which are consistent with one another within the uncertainty range. The Amoco samples yield thermal diffusivity values which are comparable to each other except for the two thinnest samples whose values are far smaller.

Equation 2 decays essentially completely before $f^2(t)$ undergoes any significant change. This is the simplest case since the signal is described by a single exponential decay giving the in-plane thermal diffusivity. In practice, since $f^2(t)$ can be approximated by an exponential [18], the thermal decay data at almost all wavevectors can be well described by a single exponential function. Decay rates, determined from the slope of ln $\eta(t)$, are plotted versus q^2 to yield a line whose slope is $2D_T$ and whose y-intercept is related to the out-of-plane heat flow rate. Fig. 6a and b show the q^2 dependence of the measured signal decay rates in 6FDA–APBP films with various thicknesses. Their in-plane thermal diffusivities are listed in Table II and are found to be consistent with results previously reported [19]. It is noted that at the two lowest q values in the thinnest (2.86 and 2.99 μm) samples, the decays are no longer exponential. This may be due to more rapid thermal diffusion into the air from both sides of these samples. An experiment conducted in one of the films in vacuum showed a significantly slower decay rate. In calculating thermal diffusivity values, the four data sets in which the decays were non-exponential were discarded.

In general, the films show more variation in thermal diffusivity values than in mechanical properties. This is also the case for spot-to-spot variations within a single film, which are comparable to the variations between films at large q values. The variations observed are outside the range of uncertainties of the measurements, and therefore it is believed that they reflect genuine variation within and among the films. Small variations in polymer morphology may be reflected more distinctly in the thermal diffusion rates (which ultimately reflect anharmonic parts of the microscopic polymer potential energy surfaces) than in the mechanical properties (which reflect the harmonic parts of the polymer potential). Alternately, variations in surface roughness may have little effect on elastic properties, but measurable influence on heat flow into the air. As shown in Fig. 6 and Table II, there is no systematic relation between the measured thermal diffusivities and film thicknesses.

4. Conclusions

The elastic and thermal properties of 4,4′-(hexafluoroisopropylidene)–*bis*(phthalic anhydride)-4,4′-*bis* (4-aminophenoxy) biphenyl (6FDA–APBP) freestanding polyimide films with various thicknesses in the 2–10 μm range have been determined through ISTS. It is found that an isotropic model of stressed unsupported films can account for the observed elastic behaviour. Young's modulus and Poisson's ratio were determined to be 2.7 ± 0.3 GPa and 0.38 ± 0.03, respectively. Thermal diffusivities showed significant sample-to-sample variations from 0.120 to 0.192 $\mu m^2 \mu s^{-1}$. Both the elastic and thermal properties of fabricated 6FDA–APBP films appear to be independent of thickness.

Acknowledgements

This work was supported in part by NSF grant no. CHE-8951738 which provided initial equipment for an undergraduate picosecond laser spectroscopy laboratory; NSF grant no. DMR-9317198; and the Donors of the Petroleum Research Fund, administered by the American Chemical Society. We wish to acknowledge full or partial donations of equipment from Tektronix, Coherent Laser, Con-Optics, Antel and Neslab. We thank Herbert Neuhaus and Paul Sanchez at Amoco Research Center, and Fred Trusell at MIT for providing samples.

References

1. A. R. DUGGAL, J. A. ROGERS and K. A. NELSON, *J. Appl. Phys.* **60** (1992) 692.
2. J. A. ROGERS and K. A. NELSON, *ibid.* **75** (1994) 1534.
3. J. A. ROGERS, Y. YANG, K. A. NELSON, *Appl. Phys. A: Solids and Surfaces* **58** (1994) 523.
4. J. A. ROGERS, L. DHAR and K. A. NELSON, *Appl. Phys. Lett.* **65** (1994) 312.
5. J. A. ROGERS and K. A. NELSON, *J. Adhes.* **50** (1995) 1.
6. J. A. ROGERS, C. MINDAS, Y. YANG and K. A. NELSON, *Mater. Res. Soc. Symp. Proc.* **323** (1993) 425–433. (We note that the actual thermal diffusivities should be twice the values reported in this paper.)
7. E. O. SHAFFER, II and S. D. SENTURIA, "The EPP databook, a compendium of research results of the MIT Electronics Packaging Program (EPP) for the years 1991–1993" (MIT, Cambridge, MA, 1993).
8. H. ROBBINS and B. SCHWARTZ, *J. Electrochem. Soc.* **107** (1960) 108.
9. F. MASEEH, M. A. SCHMIDT, M. G. ALLEN, and S. D. SENTURIA, in "IEEE solid-state sensor and actuator workshop" (Hilton Head, SC; 1988).
10. F. MASEEH and S. D. SENTURIA, in "Polyimides: materials, chemistry, and characterization", edited by C. Feger, M. M. Khojasteh and J. E. McGrath (Elsevier, Amsterdam, 1989), p. 575.
11. J. A. ROGERS and K. A. NELSON in Proceedings of the Society of Photo-Optical Instrumentation Engineers Conference OE-LASE, Vol. 1861 (1993) p. 314.
12. B. A. AULD, "Acoustic fields and waves in solids", Vol. 2 (Wiley, New York, 1973).
13. I. VIKTOROV, "Rayleigh and Lamb waves, physical theory and applications" (Plenum, New York, 1967).
14. J. A. ROGERS and K. A. NELSON, in "IEEE Trans. UFFC", in press.
15. Amoco Chemical, "Ultradel 4212 coating" (Ultradel Microelectronic Coatings).
16. A. L. FETTER and J. D. WALECKA, "Theoretical mechanics of particles and continua" (McGraw Hill, New York, 1980).
17. C. D. MARSHALL, I. M. FISHMAN, R. C. DORFMAN, C. B. EOM, and M. D. FAYER, *Phys. Rev. B* **45** (1992) 10009.
18. C. D. MARSHALL, I. M. FISHMAN, and M. D. FAYER, *ibid.* **43** (1991) 2696.
19. J. A. ROGERS and K. A. NELSON, "Materials reliability in microelectronics IV; Proc. Spring 1994 Mater. Res. Soc. Mtg., Symp." Vol. 338, edited by C. P. Borgesen, J. E. Sanchez Jr, J. C. Coburn, K. Rodbell and W. Filter p. 553 (We note that the actual thermal diffusivities should be twice the values reported in this paper.)

Received 6 March
and accepted 24 May 1995